

Description of the China global Merged Surface Temperature version 2.0

Wenbin Sun^{1,#}, Yang Yang^{1,#}, Liya Chao^{1,#}, Wenjie Dong^{1,#}, Boyin Huang², Phil Jones³,

Qingxiang Li^{1,#}

¹ School of Atmospheric Sciences and Key Laboratory of Tropical Atmosphere-Ocean System, Sun Yat-sen University, Ministry of Education, Guangzhou, China

² National Centers of Environmental Information, NOAA, Asheville, USA

³ Climate Research Unit, University of East Anglia, Norwich, UK

[#] Current address: Southern Laboratory of Ocean Science and Engineering (Guangdong Zhuhai), Zhuhai, China

Corresponding to: Qingxiang Li (liqingx5@mail.sysu.edu.cn)

Abstract. Global surface temperature observational datasets are the basis of global warming studies. In the context of increasing global warming and frequent extreme events, it is essential to improve the coverage and reduce the uncertainty of global surface temperature datasets. The China global Merged Surface Temperature Interim version (CMST-Interim) is updated to CMST 2.0 in this study. The previous CMST datasets were created by merging the China global Land Surface Air Temperature (C-LSAT) with sea surface temperature (SST) data from the Extended Reconstructed Sea Surface Temperature version 5 (ERSSTv5). The CMST2.0 contains three variants: CMST2.0-Nrec (without reconstruction), CMST2.0-Imax, and CMST2.0-Imin (According to their reconstruction area of the air temperature over the sea ice surface in the Arctic region). The reconstructed datasets significantly improve data coverage, whereas CMST2.0-Imax and CMST2.0-Imin have improved coverage in the Northern Hemisphere, up to more than 95%, and thus increased the long-term trends at global, hemispheric, and regional scales from 1850 to 2020. Compared to CMST-Interim, CMST2.0-Imax and CMST2.0-Imin show a high spatial coverage extended to the high latitudes and are more consistent with a reference of multi-dataset averages in the polar regions. The CMST2.0 datasets presented here are publicly available at the website of figshare, <https://doi.org/10.6084/m9.figshare.16929427.v4> (Sun and Li, 2021a) and the CLSAT2.0 datasets can be downloaded at <https://doi.org/10.6084/m9.figshare.16968334.v4> (Sun and Li, 2021b), and both also are available at: [http:// www.gwpu.net](http://www.gwpu.net).

1. Introduction

Global Surface Temperature (GST) is a key meteorological factor in characterizing climate change and has been widely used for climate change detection and assessment (IPCC, 2013; 2021). GST consists of global Land Surface Air Temperature (LSAT), which is the 2-m air temperature observed by land weather stations, and Sea Surface Temperature (SST) observed by ships, buoys and Argos. However, there are large uncertainties in the temperature data observed by weather stations, ships, buoys and Argos in long-term observations, including uncertainties due to uneven

38 spatial and temporal distribution of sampling (Jones et al., 1997; Brohan et al., 2006) and
39 uncertainties due to stations, environment and instrumentation changes (Parker et al., 1994; Parker,
40 2006; Trewin, 2012; Kent et al., 2017; Menne et al., 2018; Xu et al., 2018). Nevertheless, several
41 countries and research teams have applied different homogenization methods to generate a series of
42 representative homogenized global land-sea surface temperature gridded datasets, including the Met
43 Office Hadley Centre/Climatic Research Unit Global Gridded Monthly Temperature (HadCRUT)
44 (Morice et al., 2012), Goddard Institute for Space Studies Surface Temperature (GISTEMP)
45 (Hansen et al., 2010; Lenssen et al., 2019), NOAA's NOAA Global Temperature
46 (NOAAGlobalTemp) (Vose et al., 2012; Zhang et al., 2019; Huang et al., 2020), and Berkeley Earth
47 (BE) (Rohde et al., 2013a; Rohde and Hausfather, 2020), which serve as benchmark data for
48 monitoring and detecting GST changes and related studies.

49 However, there are still uncertainties in these datasets, including those due to insufficient
50 coverage, especially at high altitudes and in the polar regions (Wang et al., 2018) (~~Wang et al., 2017~~).
51 The Arctic has high climate sensitivity (Lu and Cai, 2009, 2010; Yamanouchi, 2011; Dai et al., 2019;
52 Xiao et al., 2020; Latonin et al., 2021), the absence of data for this region would lead to a cold bias
53 in the estimated global mean surface temperature (GMST). How to ~~improve-account for~~ this
54 deficiency is an issue that must be addressed to optimize and improve the observations. Since IPCC
55 AR5 (2013), all ~~of~~ the above datasets have been updated and reconstructed in the data default region
56 (IPCC, 2021). For example, Cowtan and Way (2014) used kriging and hybrid methods to fill in the
57 HadCRUT4 data gap areas, extending the data to polar regions. GISSTEMP v4 utilized spatial
58 interpolation methods to fill in the default data within the appropriate distances (1200km) (Lenssen
59 et al., 2019). NOAA/NCEI used spatial smoothing and empirical orthogonal remote correlations
60 (EOTs) to reconstruct the data default areas, generating 100-member GHCN ensemble data and
61 1000-member ERSST ensemble data, respectively, which were combined into the
62 NOAAGlobalTemp-Interim dataset (Vose et al., 2021). HadCRUT team infilled HadCRUT5 using
63 the Gaussian process method (Morice et al., 2021). Kadow et al. (2020) used artificial intelligence
64 (AI) in combination with numerical climate model data to fill the observation gaps in HadCRUT4.
65 Berkeley Earth used kriging-based spatial interpolation to fill in the terrestrial default data (Rohde
66 et al., 2013a; Rohde et al., 2013b; Rohde and Hausfather, 2020). Interpolation and reconstruction
67 for high latitudes reduce the error in the estimate of GMST. Compared to 0.61 (0.55-0.67) °C in
68 IPCC AR5, GST warming estimated with reconstructed datasets in AR6 from 1850-1800 to 1986-
69 2005 is 0.69 (0.54-0.79) °C, which increased 0.08 (-0.01 to 0.12) °C (IPCC, 2021).

70 China global Merged Surface Temperature (China-MST or CMST) is a new global surface
71 temperature dataset developed by the team at Sun Yat-sen University, which was ~~generated by~~
72 ~~merged by~~ China global Land Surface Air Temperature (China-LSAT or C-LAST) (Xu et al.,
73 2018; Yun et al., 2019; Li et al., 2020; Li et al., 2021) as the terrestrial component and ERSSTv5
74 (Extended Reconstructed Sea Surface Temperature version 5) (Huang et al., 2017) as the ocean
75 component. It is generally consistent with other global datasets in terms of GST trends and
76 uncertainty levels since 1880 (Li et al., 2020). ~~Both the CMST and C-LSAT datasets have a~~
77 ~~resolution of 5° × 5° in the latitude and longitude directions.~~ Compared with other datasets,
78 the station coverage of C-LSAT has been significantly improved, especially for Asia (Xu et al.,
79 2018), and more ISTI station data have been added in C-LSAT 2.0 (Li et al., 2021; Thorne et al.,
80 2011). In addition, C-LSAT adopted a homogenization scheme for temperature series that is different

81 from datasets such as the Global Historical Climatology Network version 4 (GHCNm v4)(Menne
82 et al., 2018; Li et al., 2022)-(Menne et al., 2018; Li et al., 2022). Further, Sun et al. (2021) trained
83 EOTs modes with “state-of-the-art” ERA5 reanalysis data to extract the spatial distribution of LSAT.
84 They then used a similar low- and high-frequency reconstruction method of Huang et al. (2020)
85 with different parameter schemes, combined with the observation constraint method, to fill the data
86 default region of C-LSAT2.0 and released the new reconstructed dataset C-LSAT2.0 ensemble and
87 the global surface temperature dataset CMST-Interim. Compared with the original CMST, CMST-
88 Interim significantly improves the coverage of GST, and the GST warming estimated by CMST-
89 Interim is more significant, with the warming trend since the 1900s increasing from $0.085 \pm 0.004^{\circ}\text{C}$
90 $(10 \text{ yr})^{-1}$ to $0.089 \pm 0.004^{\circ}\text{C}$ $(10 \text{ yr})^{-1}$. In the current CMST-Interim (Sun et al., 2021) and its earlier
91 version (Yun et al., 2019), we still fully adopted the setting from ERSSTv5, which treats the sea ice
92 region in the Arctic as the sea surface temperature below the sea ice and assigns a default value (-
93 1.8°C), which makes it still a gap in the polar region. In contrast, polar regions are susceptible to
94 climate forcing, with the Arctic warming more than twice the global average in recent decades
95 (Goosse et al., 2018). The lack of data from CMST-Interim in polar regions may result in a slight
96 underestimation of its estimated global warming trend. Furthermore, CMST-Interim does not
97 systematically assess the reconstruction uncertainty of LSAT, resulting in an incomplete estimate of
98 global surface temperature uncertainty (Li et al., 2021). Although C-LSAT 2.0 ensemble satisfied
99 the criterion of the recently released the 6th assessment report of IPCC, the CMST -Interim does not
100 appear in the core assessment GMST series due to its insufficient data coverage in the Arctic region
101 (Gulev et al., 2021)(Gulev et al., 2021).

102 To address the above issue and improve coverage of CMST in the Arctic, we further reconstruct
103 and supplement the Arctic data default region in the dataset using a combination of statistical
104 interpolation and high- and low-frequency reconstruction to develop the reconstructed CMST2.0
105 dataset and assess its uncertainty. Section 2 introduces the update of terrestrial and oceanic datasets,
106 section 3 presents the reconstruction and uncertainty analysis of CMST2.0, section 4 introduces the
107 composition of C-LSAT2.0 and CMST2.0, section 5 analyzes the GMST series of CMST2.0, section
108 6 is the comparison of CMST2.0 dataset with other datasets, section 7 provides the summary and
109 outlook, and section 8 is data availability.

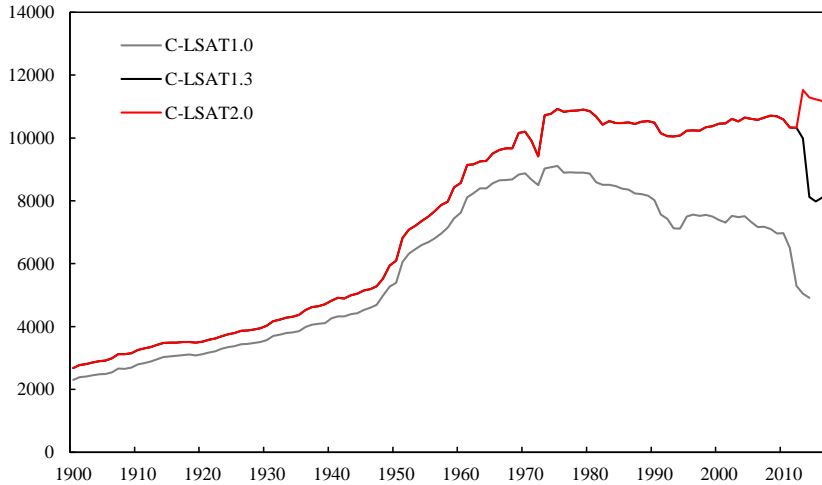
110 2. Updates of the land and ocean datasets

111 2.1 Data sources and initial processing for C-LSAT2.0

112 The initial version of the C-LSAT dataset was C-LSAT1.0. The C-LSAT1.0 site dataset
113 collected and integrated 14 LSAT datasets, including three global data sources (CRUTEM4, GHCN-
114 V3, and BEST), three regional data sources, and eight national situ data sources (Xu et al., 2018).
115 The current latest version is C-LSAT 2.0 (Li et al., 2021; Sun et al., 2021).

116 C-LSAT 2.0 used in this study is an update of C-LSAT 1.3. Compared to C-LSAT 1.3 from
117 1900 to 2017, version 2.0 extend to 1850-2020, and there is a significant increase in the amount of
118 in situ data for the period 2013-2017 (Figure 1), with the increased situ data from CLIMAT from
119 WMO’s Global Telecommunication System (GTS) and Global Surface Daily Summary (GSOD)
120 (<https://www.ncei.noaa.gov/data/global-summary-of-the-day/archive/>; last access: November 2021)
121 and is homogenized using the same method as Xu et al. (2018). In addition, we have updated the
122 data in C-LSAT2.0 for 2013-2019, which adds the number of situ data in Africa, North America and
123 other regions in this study. The C-LSAT 2.0 dataset includes three temperature elements: monthly
124 mean temperature, maximum temperature, and minimum temperature, and its time range for the

125 three elements is January 1850 - December 2020.



126
127 Figure 1 Comparison of C-LSAT 1.3 and C-LSAT 2.0 site counts from 1900 to 2017

128 2.2 Sea surface temperature

129 CMST1.0 (Yun et al., 2019) and CMST-Interim (Sun et al., 2021) use ERSSTv5 as the ocean
130 component (Huang et al., 2017). ERSSTv5 starts from 1854, and we extend ERSSTv5 (1854-present)
131 to 1850 using 1850-1853 SST anomalies (relative to 1961-1990 average) from ICOADS Release
132 3.0 (Freeman et al., 2017) and integrated into a global SST anomaly dataset for January 1850 -
133 December 2020. In the above integrated SST dataset, the SST is still set to a constant value of -
134 1.8°C for areas with >90% sea ice coverage as ERSSTv5. In addition, some areas in the high
135 latitudes of the Southern Hemisphere (non-sea ice) are marked as missing values due to the lack of
136 observations.

137 2.3 Sea ice surface air temperature

138 The common air temperature observation for the Arctic region is The International Arctic Buoy
139 Program (IABP) (http://research.jisao.washington.edu/data_sets/iabppoles/; last access: October
140 2021), which contains oceanographic and meteorological observations for the Pacific Arctic, but it
141 only has sea ice data from 1979 to the present, while the climate state of CMST is ~~1969-1998~~[1961-](#)
142 [1990](#), the time length of IABP does not support us to estimate and reconstruct the temperature
143 anomaly of the Arctic region in the CMST dataset, so we use the [Adjusted](#) Inverse Distance
144 Weighted ([AIDW₂](#) (Cheng et al., 2020)) extrapolation (site data) and EOT interpolation (gridding)
145 methods to fill the default grid of the polar region (Cowtan and Way, 2014; Lenssen et al., 2019;
146 Rohde and Hausfather, 2020; Vose et al., 2021).

147 3. CMST2.0 reconstruction and uncertainty analysis

148 3.1 CMST and its brief reconstruction history

149 CMST 1.0 consists of C-LSAT 1.3 (1900-2017) as the terrestrial component and ERSSTv5 as
150 the ocean component. The latest version without reconstruction is CMST2.0-Nrec in this study,
151 which composes of C-LSAT2.0 and ERSSTv5. Compared to CMST1.0 from 1900-2017, CMST2.0-
152 Nrec has been updated and expanded to 1850-2020. The original reconstructed version of CMST is
153 the Chinese global merged surface temperature reconstruction dataset CMST-Interim, which is a

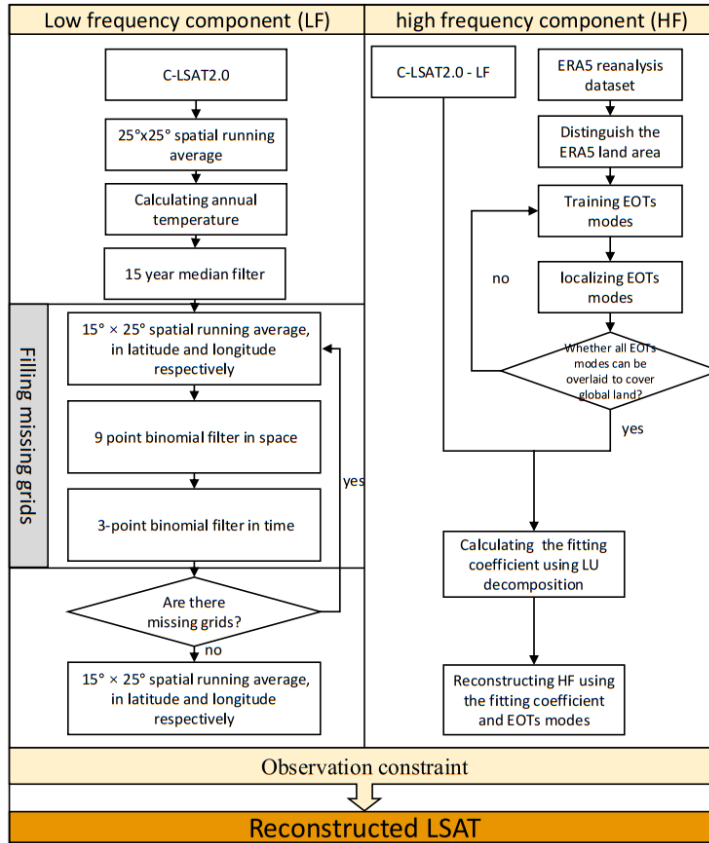
154 merge of the reconstructed C-LSAT2.0 and ERSSTv5, where the reconstructed C-LSAT2.0 is an
155 ensemble reconstruction dataset upgraded from C-LSAT2.0 (Li et al., 2021) with 756 ensemble
156 members identified based on EOT and smoothing (Sun et al., 2021). Considering that there are much
157 missing data due to sea ice coverage at high latitudes in the Northern Hemisphere in CMST, the
158 [AIDW](#) extrapolation method is proposed to infill the missing data in some key sites, then EOT
159 interpolation method is used to reconstruct all the grid boxes over the sea-ice-covered region in this
160 paper. Considering the effect of interannual variability of sea ice in the Arctic, 65°N-90°N and 80°N-
161 90°N are taken as the assumed land components for ensemble reconstruction with C-LSAT 2.0,
162 respectively, using the maximum sea ice area and minimum sea ice area since satellite observations
163 are available as reference, then the ERSSTv5 ensemble reconstruction dataset is merged to generate
164 CMST 2.0-Imax and CMST 2.0-Imin datasets.

165 **3.2 Reconstruction of terrestrial and marine components**

166 **3.2.1 Reconstruction of the terrestrial component**

167 We follow the reconstruction method of CMST-Interim (Sun et al., 2021) and divide the C-
168 LSAT 2.0 dataset into two parts, high- and low-frequency components, for reconstruction, then sum
169 them to obtain the reconstructed LSAT data (Figure 2). The low-frequency component is a running
170 average over time and space to characterize the large-scale features of LSAT anomalies in time and
171 space. First, a 25° x 25° spatial running average is performed, and then the annual average of LSAT
172 anomalies is calculated for at least two months of the year. Then, a 15-year median filter is used for
173 the annual average LSAT, followed by a 15° x 25° spatial sliding average, a 9-point binomial spatial
174 filter, and a 3-point binomial temporal filter for latitude and longitude, respectively, to fill in the
175 default data. Finally, a 15° x 25° spatial running average is applied to latitude and longitude
176 respectively to smooth the spatial distribution of the LSAT. The high-frequency component is the
177 difference between the original data and the low-frequency component, characterizing the local
178 variation of LSAT. We train the EOTs modes using the ERA5 reanalysis dataset (Hersbach et al.,
179 2020) (<https://cds.climate.copernicus.eu/>; last access: July 2020) and localize it. Afterward, the
180 EOTs modes are used to fit the high-frequency data to obtain a full-coverage reconstruction of the
181 high-frequency component (Sun et al., 2021). The reconstructed land temperature data can be
182 obtained by summing the low-frequency and high-frequency components, and finally, the
183 reconstructed data are observationally constrained to remove the low-quality reconstructed data.

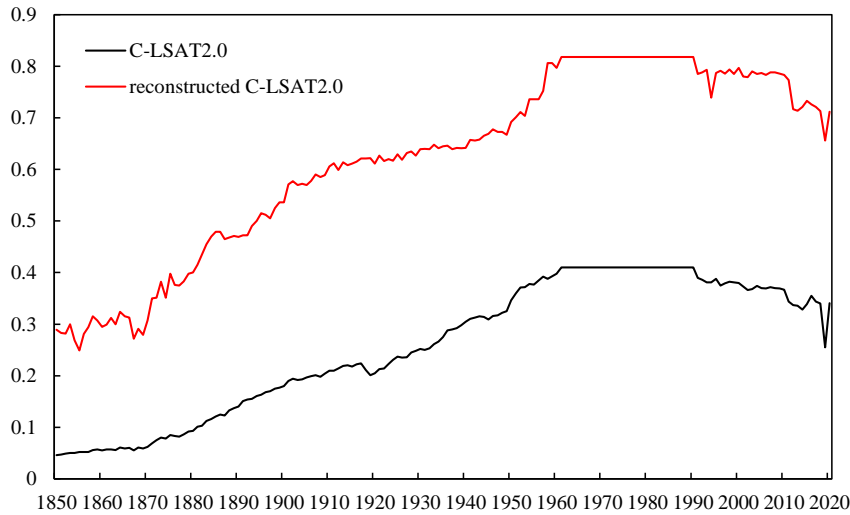
184



185
186
187
188
189
190
191
192
193

Figure 2 Schematic diagram of the LSAT reconstruction process

Reconstruction greatly improves the coverage of C-LSAT2.0. Figure 3 shows the comparison of land coverage before and after reconstruction. The land coverage of the reconstructed C-LSAT2.0 increases from the original 4.6% in 1850 to 29%, and the land coverage remains above 60% after 1913 and reaches the maximum land cover of about 80% in 1961, which last until 1990, after which it slightly decreases and remains at about 78%. After 2012 there is a decreasing trend to about 70%, where the land cover in 2019 is the lowest value of 66% for the period 2012-2020, this is related to the lower number of sites in the year.



194

Figure 3 Coverage comparison of the terrestrial component before and after reconstruction

195

196

3.2.2 Reconstruction of the ocean component

197

We use ERSSTv5 data as the basis, which is a full-coverage, monthly reconstructed SST dataset based on observations from ships, buoys, and Argo (Huang et al., 2017). We fill the data during 1850-1853 with SST anomaly observed by ICOADS Release 3.0 (Freeman et al., 2017) to form a complete monthly SST anomaly dataset from 1850-2020 and then reconstruct it using the EOTs of Huang et al. (2017) to reduce the missing data.

198

199

200

201

202

3.3 Reconstruction of Arctic ice surface temperature

203

In CMST-Interim, when the Arctic is covered by sea ice, ERSSTv5 sets SST in the region with >90% sea ice coverage to a constant value (-1.8°C), making ST of CMST-Interim in the polar region the default value. It is worth noting that the Arctic is extremely sensitive to changes in climate forcing (polar amplification effect), so missing data in the polar regions in CMST-Interim may lead to an underestimation of the global warming trend (IPCC, 2021).

204

205

206

207

208

In order to solve this problem and improve the coverage of CMST in the Arctic, we improve the ST reconstruction method in the Arctic by expressing the ST of the Arctic in terms of the air temperature of ice surface (considering the similar physical properties of ice and land, the sea ice is considered as the land). The month with the largest extent of Arctic sea ice is March, and the month with the smallest extent is September. According to the National Snow and Ice Data Center, during 1980-2020, the year with the largest sea ice extent in March is 1983 and the year with the smallest sea ice extent in September is 2012, so we designed two experiments: 1) CMST2.0-Imax uses 2 m air temperature to represent the temperature within the 65°N-90°N region to simulate the ST of the Arctic sea ice-covered region in March 1983, which is the maximum sea ice extent. 2) CMST2.0-Imin uses 2 m air temperature to represent the temperature within the 80°N-90°N region to represent the ST in the Arctic sea ice-covered region at the time of September 2012, which is the minimum sea ice extent (Figure 4).

209

210

211

212

213

214

215

216

217

218

219

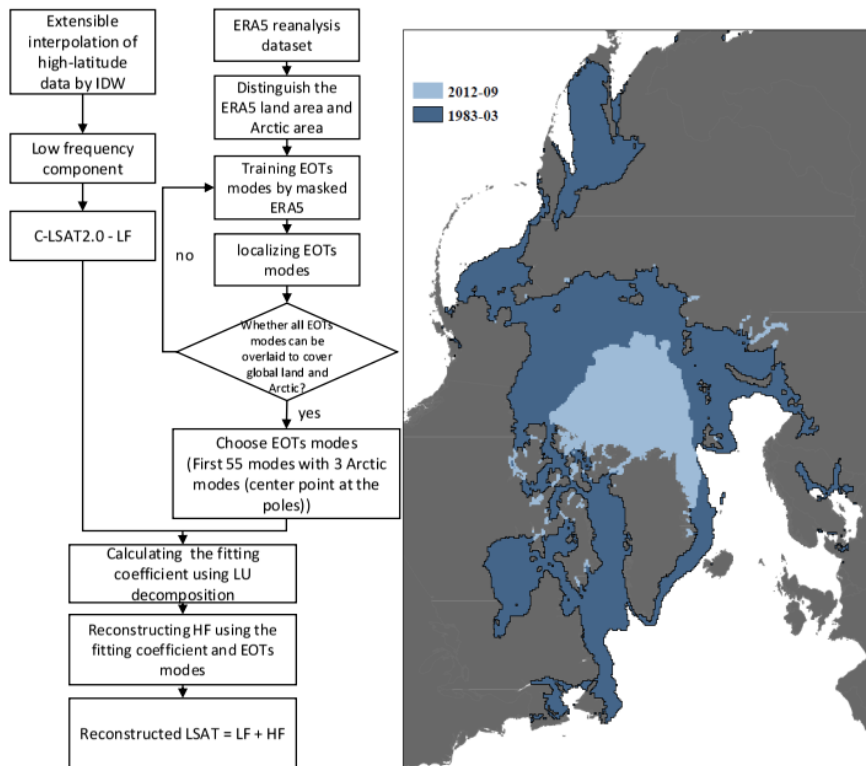


Figure 4 Reconstruction process of Arctic sea ice ST (left); comparison of maximum sea ice extent (sea ice extent in March 1983, shaded in dark blue) and minimum sea ice extent (sea ice extent in September 2012, shaded in light blue) distribution (right)

3.3.1 Maximum sea ice extent reconstruction CMST2.0-Imax

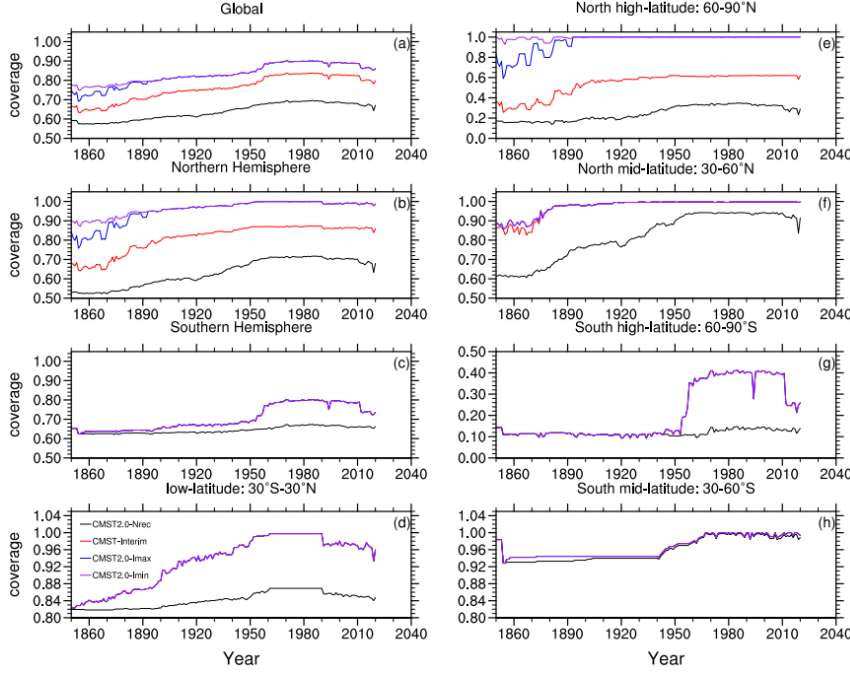
Due to the scarcity of observations in the Arctic and the fact that most observations were available after the 1980s, the observation period is very short. The data do not cover all the period of 1961-1990, which is the climatology of our dataset. Therefore the observations cannot be added to the C-LSAT 2.0 dataset. Due to this fact, we use the [Inverse Distance Weighted method \(IDW\)](#) (Cheng et al., 2020) to interpolate the data at lower latitudes to the Arctic (65°N-90°N) and then perform the high- and low-frequency reconstruction method based on the interpolated dataset. It is worth noting that we included the region of 65°N-90°N when training EOTs using the ERA5 reanalysis dataset. We selected the first 55 modes of the EOTs with three polar modes (the center point at the Arctic poles), for a total of 58 modes for reconstructing the high-frequency components (Figure 4). After that, the reconstructed C-LSAT is merged with ERSSTv5, where the merged ERSSTv5 covers only the region south of 65°N.

3.3.2 Minimum sea ice extent reconstruction CMST2.0-Imin

The reconstruction method of the terrestrial component in CMST2.0-Imin is consistent with CMST2.0-Imax, except that the merged process with ERSSTv5, in CMST2.0-Imin, the merged ERSSTv5 coverage is south of 80°N. It is worth noting that the sea ice coverage range is 80°N-90°

240 N and the region of 65°N-80°N fill in SST in CMST2.0-Imin. However there are some grids in the
241 region of 65°N-80°N that are default values (caused by sea ice coverage) in ERSSTv5, so we use
242 the [AIDW](#) method to fill these default grids.

243 Figure 5 shows the coverage comparison of CMST2.0-Nrec (without any land and ice air
244 temperature reconstruction), CMST-Interim, CMST2.0-Imax, and CMST2.0-Imin. Overall, there is
245 a significant improvement in the coverage of the reconstructed datasets compared to the original
246 dataset, CMST2.0-Nrec. Globally, the coverage of CMST2.0-Imax and CMST2.0-Imin
247 reconstructed for Arctic sea ice is consistently higher than CMST-Interim. CMST2.0-Imax and
248 CMST2.0-Imin have the highest global coverage, with >80% coverage after 1899. The global
249 coverage of CMST-Interim reached more than 80% after 1957. The comparative results for Northern
250 Hemisphere coverage are primarily consistent with the global, with CMST2.0-Imax and CMST2.0-
251 Imin having the greatest coverage, both reaching more than 90% after the 1880s, and CMST-Interim
252 reaching 80% coverage in 1901, but consistently below 90%. In terms of global and Northern
253 Hemisphere coverage, there are differences between CMST2.0-Imax, CMST2.0-Imin, and CMST-
254 Interim, but the differences are not significant. However, the coverage of CMST2.0-Imax and
255 CMST2.0-Imin differed significantly from CMST-Interim at high latitudes in the Northern
256 Hemisphere, where the coverage of CMST-Interim has been below 70% due to the existence of sea
257 ice, while CMST2.0-Imax and CMST2.0-Imin ~~reach~~ reach full coverage at high latitudes in the
258 Northern Hemisphere after 1983. There is no difference in the coverage of the three reconstructed
259 datasets in other regions (Southern Hemisphere, Southern Hemisphere mid-high and low latitudes)
260 except for the Northern Hemisphere and Northern Hemisphere high latitudes. The coverage of the
261 reconstructed dataset in the Southern Hemisphere has improved considerably, with a maximum
262 coverage of about 80%. The coverage of the reconstructed dataset in the high latitudes of the
263 Southern Hemisphere is relatively small, consistently below 50%, due to the scarcity of observations
264 in Antarctica.



265
 266 Figure 5 Coverage comparison of CMST2.0-Nrec, CMST-Interim, CMST2.0-Imax and CMST2.0-
 267 Imin

268 3.4 Estimation of uncertainty in the reconstructed CMST2.0

269 Uncertainties of the reconstructed CMST2.0 include both land and ocean uncertainties. The
 270 ocean uncertainty is the uncertainty of ERSSTv5. The land uncertainty is based on the reconstructed
 271 C-LSAT2.0 ensemble, which is divided into two parts: parameter uncertainty and reconstruction
 272 uncertainty. Since we reconstruct the temperature of the polar sea ice region in the way that we
 273 reconstruct the LSAT, we calculate the uncertainty of the 65°N-90°N (Imax) and 80°N-90°N (Imin)
 274 regions of CMST2.0-Imax and CMST2.0-Imin following the method of calculating the land
 275 uncertainty.

276 3.4.1 Parameter uncertainty of C-LSAT2.0 ensemble

277 In the reconstruction process, we choose different parameters to generate 756-member
 278 ensembles (Table 1), which are different for different combinations, so the parameter uncertainty
 279 represents the difference of parameter combinations. According to Huang et al. (2020), the
 280 parameter uncertainty (U_p) is the regional average LSAT uncertainty, as follows:

$$U_p^2(t) = \frac{1}{M} \sum_{m=1}^M [A_m^g(t) - \overline{A^g}(t)]^2 \quad (1)$$

$$\overline{A^g} = \frac{1}{M} \sum_{m=1}^M A_m^g(t) \quad (2)$$

281 where M is the ensemble member, in this paper M=756; A_m^g represents global LSAT of m-member

282 ensemble; $\overline{A^g}$ is the average of all ensembles; t represents temporal variations.

283 Table 14 Parameter settings used for reconstruction scenarios and the operational option.

PARAMETER	OPERATIONAL OPTIONS	ALTERNATIVE OPTIONS
MINIMUM NUMBER OF MONTHS ANNUAL AVERAGE	2 months	1, 2, 3 months
LF FILTER PERIODS	15 years	10, 15, 20 years
MIN NUMBER OF YEARS FOR LF FILTER	2 years	1, 2, 3 years
EOTS TRAINING PERIODS AND SPATIAL SCALES	1979-2018, Lx=4000, 3000, 2500, Ly=2500	1979-2018, Lx=3000,2000,1500, Ly=1500; 1979-2018, Lx=5000,4000,3500, Ly=3500; Lx=4000,3000,2500, Ly=2500; 1979-2008, Lx=4000,3000,2500, Ly=2500; 1989-2018, Lx=4000,3000,2500, Ly=2500; even year, Lx=4000, 3000, 2500, Ly=2500; odd year, Lx=4000, 3000, 2500, Ly=2500;
EOTS ACCEPTANCE CRITERION	0.2	0.10, 0.15, 0.20, 0.25

格式化表格

284 Parameter uncertainties for the reconstructed C-LSAT2.0 ensemble, reconstructed C-
285 LSAT2.0+Imax (65°N-90°N) and reconstructed C-LSAT2.0+ Imin (80°N-90°N) show similar
286 variations. The parameter uncertainties decreases over time, as does its interannual variability. The
287 parameter uncertainties stabilizes below 0.05 during 1876-2016 (Figure 7). However, the parameter
288 uncertaintyies areis higher in 2018-2020 compared to the previous years. This is due to the lower
289 coverage in this period compared to the last years, which is more sensitive to the parameter settings.

290 3.4.2 Reconstruction uncertainty of C-LSAT2.0 ensembles

291 In the reconstruction process, we smooth the observations when calculating the low-frequency
292 component to filter out the short-term and local signals to obtain the large-scale characteristics of
293 the LSAT anomaly, after which the high-frequency component is used to fit the local distribution of
294 LSAT using the EOTs spatial modes and the available observations. Our purpose of using EOTs is
295 to obtain the spatial distribution of the LSAT anomaly, filter out the errors in the observations, and
296 thus estimate the distribution of the LSAT anomaly from limited observations. However, the spatial
297 pattern of EOTs also smoothes out the local temperature and ignores some local information, thus
298 deviating from the observations. Therefore, according to Huang et al. (2016), we define the residual
299 between the ideal observations and the reconstructed values using EOTs as the reconstruction
300 uncertainty:

$$U_r^2(t) = \frac{1}{M} \sum_{m=1}^M [R_m^g(t) - D(t)]^2 \quad (3)$$

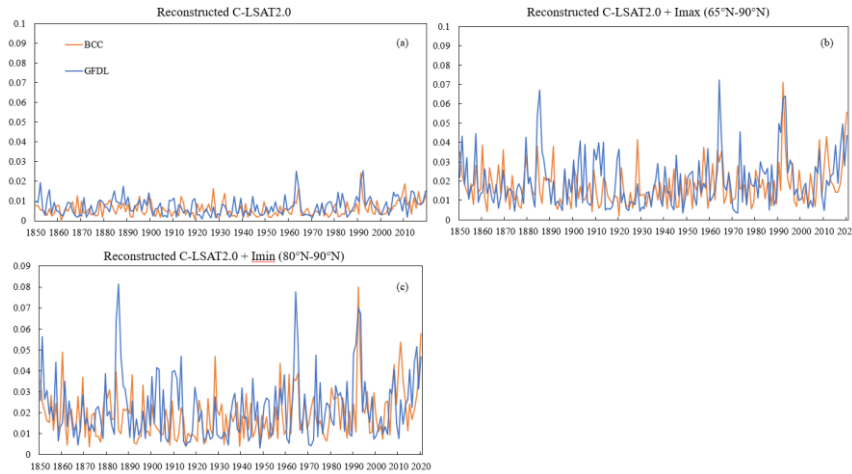
301 where $D(t)$ represents the ideal observation and $R_m^g(t)$ is the reconstructed data obtained using
302 the high- and low-frequency reconstruction method based on $D(t)$.

303 The reconstruction uncertainty represents the differences between the ideal observations and
304 the reconstructions. We choose two full-coverage CMIP6 models to represent the ideal observations
305 to assess the deviation of the reconstructed values from the original values, which is due to missing
306 information caused by the smoothing of local temperatures by EOTs. The C-LSAT 2.0 ensemble
307 dataset covers the period 1850-2020, while the CMIP6 model historical experimental data are only

308 available up to 2014, so we use model data from the SSP370 scenario (taking into account minor
 309 differences in the short term for any scenarios) to complement that of 2015-2020.

310 The two models we selected are BCC-CSM2-MR and GFDL-ESM4. BCC-CSM2-MR is a new
 311 version of the climate system model developed by the National Climate Center of China with
 312 improved parameterization and physical parameterization results. GFDL-ESM4 is an Earth system
 313 model developed by the GFDL model of NOAA's Geophysical Fluid Dynamics Laboratory. Both
 314 models have a resolution of $1.125^\circ \times 1.125^\circ$, and we descale both to $5^\circ \times 5^\circ$ to calculate the
 315 temperature anomaly (1961-1990 climatology), after which the data from both models are
 316 reconstructed according to the high- and low-frequency reconstruction method.

317 Figure 6 shows the reconstruction uncertainties calculated using BCC-CSM2-MR and GFDL-
 318 ESM4. In general, the reconstruction uncertainties are relatively stable, do not increase over time.
 319 The reconstruction uncertainties of reconstructed C-LSAT2.0+Imax and reconstructed C-LSAT2.0+
 320 Imin are larger than that of reconstructed C-LSAT2.0, and the interannual variation is also larger.
 321 The interannual variability of the uncertainty of BCC-CSM2-MR is slightly smaller than that of
 322 GFDL-ESM4. In the following, we choose BCC-CSM2-MR as the reconstruction uncertainty to
 323 discuss the uncertainty of the terrestrial component.



324
 325 Figure 6 Reconstruction uncertainty of the reconstructed C-LSAT2.0 ensemble,
 326 reconstructed C-LSAT2.0+Imax (65°N-90°N) and reconstructed C-LSAT2.0+ Imin (80°N-90°N)
 327 calculated using BCC-CSM2-MR and GFDL-ESM4.

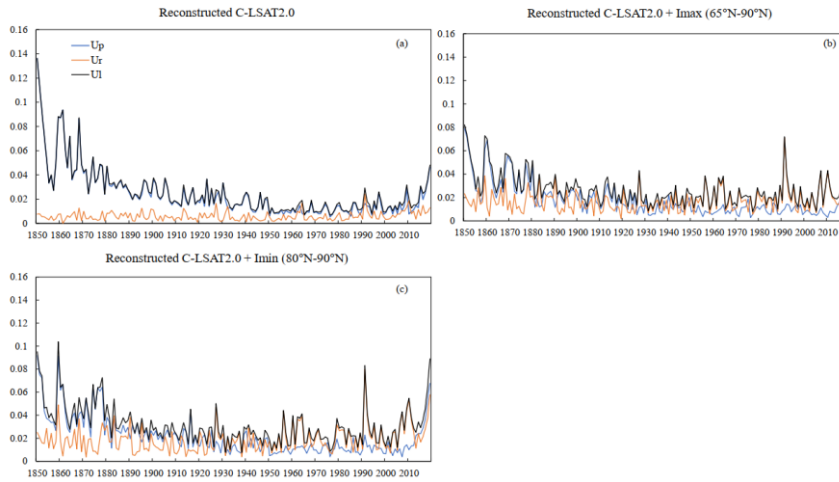
328 3.4.3 Total uncertainty of LSAT

329 The total uncertainty of the C-LSAT2.0 ensemble is the sum of the parameter uncertainty and
 330 the reconstruction uncertainty:

$$U_t^2 = U_p^2 + U_r^2 \quad (4)$$

331 Figure 7 shows the comparison of parameter uncertainty, reconstruction uncertainty and total
 332 uncertainty of three C-LSAT2.0 ensemble datasets. The parameter uncertainties of the reconstructed
 333 C-LSAT2.0 ensemble, reconstructed C-LSAT2.0+Imax (65°N-90°N) and reconstructed C-
 334 LSAT2.0+ Imin (80°N-90°N) are much larger than the reconstruction uncertainties before 1950,
 335 when the parameter uncertainties mainly determines the magnitude of total uncertainties. The

336 difference between the parameter uncertainties and the reconstruction uncertainties from 1950 ~~to~~
 337 2016 becomes small, and both determine the total uncertainties. The total uncertainties increase after
 338 2017 due to the increase in parameter uncertainties (Figure 7a). The uncertainties of reconstructed
 339 C-LSAT2.0+Imax and C-LSAT2.0+Imin vary similarly (Figure 7b&7c). The parameter
 340 uncertainties of reconstructed C-LSAT2.0+Imax and C-LSAT2.0+Imin ~~is~~ are larger than the
 341 reconstruction uncertainties before 1880, when the total uncertainties ~~is~~ are dependent on parameter
 342 uncertainties. During 1880-1950, the magnitude and variation of the parameter uncertainties and the
 343 reconstruction uncertainties are similar. After 1950, the parameter uncertainties decrease to less than
 344 the reconstruction uncertainties, during which reconstruction uncertainties determine the magnitude
 345 and variation of the total uncertainties.



346
 347 Figure 7 Parameter Uncertainty, reconstruction uncertainty and total uncertainty of three
 348 reconstructed C-LSAT2.0 ensemble

349 3.4.4 Uncertainty of global surface temperature

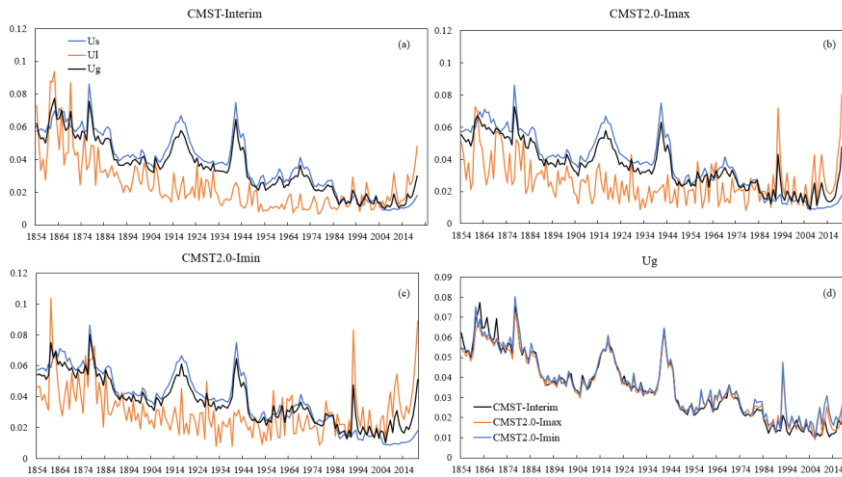
350 The uncertainty of the global surface temperature consists of two components, the ocean
 351 component and the land component, and we calculate the total global temperature uncertainty as the
 352 sum of the two, based on the sea-to-land ratio, with the following formula:

$$U_g^2 = a \times U_l^2 + b \times U_s^2 \quad (5)$$

353 where U_g represents the total uncertainty of GMST, U_l represents the uncertainty of global
 354 averaged LSAT, here chosen from the reconstructed C-LSAT2.0; U_s represents the uncertainty of
 355 global averaged ocean component, here chosen from the ERSSTv5, since the uncertainty of
 356 ERSSTv5 is only calculated up to 1854, our uncertainty of GST forward also only covers up to 1854.
 357 a and b are constants, which are the proportion of land and ocean area to the globe, respectively, but
 358 since the uncertainty of reconstructed Arctic region in CMST2.0+Imax and CMST2.0+Imin is
 359 calculated according to the land uncertainty, $a=0.32$ and $b=0.689$ in CMST2.0+Imax and $a=0.30$ and
 360 $b=0.70$ in CMST2.0+Imin.

361 Figure 8 shows uncertainties of the GMST, land component, and ocean component for CMST-
 362 Interim (a), CMST2.0+Imax (b) and CMST2.0+Imin (c). The variation in GMST uncertainty is
 363 similar for the three datasets, but the interannual variation in GMST uncertainty for CMST2.0+Imax

364 and CMST2.0-Imin is larger than CMST-Interim, especially after 1994, when both the magnitude
 365 and interannual variation in GMST uncertainty for CMST2.0-Imax and CMST2.0-Imin
 366 are significantly greater than CMST-Interim (Figure 8d). Uncertainties in the ocean and land
 367 components have generally declined, and thus the uncertainty of GMST has also reduced (Figure
 368 8a-c). Before 1870, the uncertainties of land and ocean component are similar, but the interannual
 369 variability of the land uncertainty is greater than that of the ocean. During 1871-1986, the
 370 uncertainty in the ocean component is larger than the uncertainty in the land component, and the
 371 uncertainty of GMST depended mainly on the uncertainty in the ocean component, and the
 372 interannual variability was consistent with the ocean component. There are two peaks in global
 373 uncertainty during this period, in the late 1910s and early 1940s, consistent with ocean uncertainty.
 374 The peaks in ocean uncertainty are associated with the two world wars, and the uncertainty is larger
 375 due to the smaller observation coverage of the SST during the war period(Huang et al., 2020).
 376 Between 1986 and 2003, the uncertainty of GST was determined by both the land and ocean
 377 components. After 2003, the magnitude of uncertainty of the ocean component is smaller than that
 378 of the land component, and the land component determines the magnitude of the uncertainty of GST,
 379 and the interannual variation is also consistent with the land component.



380
 381 Figure 8 Uncertainties of GMST (U_g), LSAT (U_l) and SST (U_s) for CMST-Interim (a), CMST2.0-
 382 Imax (b) and CMST2.0-Imin (c) and their comparison of U_g (d).

383 4. Composition of C-LSAT2.0 and CMST2.0

384 The C-LSAT2.0 datasets consist of two datasets, C-LSAT2.0 and reconstructed C-LSAT2.0, while
 385 each dataset includes three temperature-related elements, including monthly average, maximum,
 386 and minimum temperatures.

387 The CMST2.0 datasets consist of three versions: CMST2.0-Nrec, CMST2.0-Imax, and
 388 CMST2.0-Imin (Table 2).

389 CMST2.0-Nrec is the observation-based homogenized gridded dataset, consisting of C-
 390 LSAT2.0 and ERSSTv5, where the uncertainty of C-LSAT2.0 is not estimated, and the uncertainty
 391 of ERSSTv5 consists of parameter uncertainty and reconstruction uncertainty.

392 CMST2.0-Imax is based on CMST-Interim gridded dataset with the addition of Arctic
 393 reconstruction (65°N - 90°N), including reconstructed C-LSAT2.0 with the addition of Arctic

设置了格式: 字体: Times New Roman

394 reconstruction (65°N-90°N) and ERSSTv5 with 90°S-65°N. Its uncertainties include the terrestrial
 395 uncertainty and the oceanic uncertainty, where the terrestrial uncertainty is the uncertainty of the
 396 reconstructed C-LSAT2.0 and of the reconstructed SAT over the ice surface, including the parameter
 397 uncertainty and the reconstruction uncertainty, and the oceanic uncertainty is derived from the
 398 uncertainty of ERSSTv5 (Huang et al., 2017).

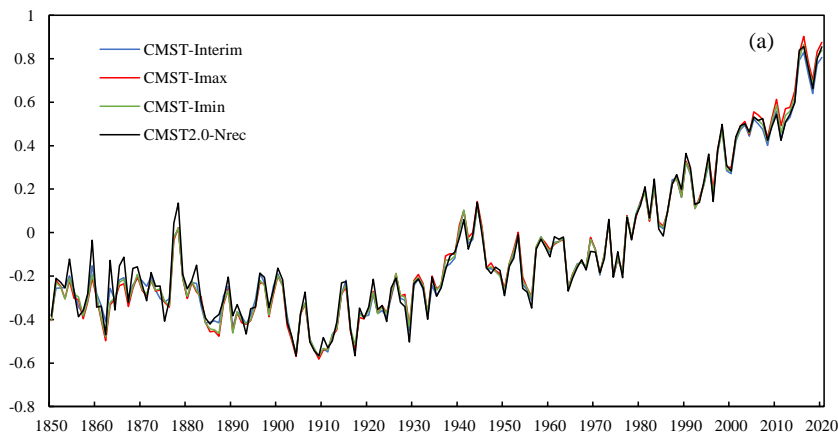
399 Similarly, CMST2.0-Imin is the gridded data, which modifies the reconstructed Arctic region
 400 based on CMST2.0-Imin. The modification part is to reduce the reconstructed Arctic region of C-
 401 LSAT2.0 to 80°N-90°N and expand the merged ERSSTv5 to 90°S-80°N area.

402 Table 22 Composition of CMST2.0 datasets and CMST-Interim.

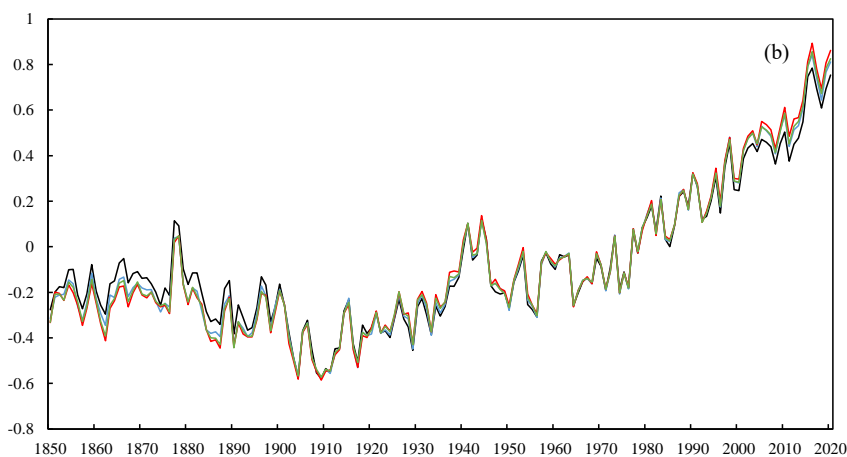
Versions	Timespan	LSAT		SST	
		datasets	uncertainty	datasets	uncertainty
CMST2.0-Nrec	1850-2020	C-LSAT2.0	—	ERSSTv5	
CMST-Interim	1850-2020	Reconstructed C-LSAT2.0		ERSSTv5	
CMST2.0-Imax	1850-2020	Reconstructed C-LSAT2.0 added Arctic reconstruction (65N-90N)	Parameter uncertainty + Reconstruction uncertainty	ERSSTv5 (90S-65N)	Parameter uncertainty + Reconstruction uncertainty
CMST2.0-Imin	1850-2020	Reconstructed C-LSAT2.0 added Arctic reconstruction (80N-90N)		ERSSTv5 (90S-80N)	

403 **5. The GMST series of CMST2.0 datasets**

格式化表格



404



405

406 Figure 9 Comparison of GMST anomalies series (relative to 1961-1990 average) for
 407 CMST2.0 datasets and CMST-Interim using two methods: a) the mean of global mean LSAT and
 408 SST weighted the proportion of land and sea.; b) calculated based on latitudinal weighting

409 Comparing the GMST series of CMST2.0 datasets and CMST-Interim shows that the variability
 410 of GMST in the reconstructed datasets is generally consistent with CMST2.0-Nrec (Figure 9). We
 411 also compare the GMST series for the four datasets calculated by the two methods, which is similar
 412 for the three reconstructed datasets (CMST-Interim, CMST2.0-Imax and CMST2.0-Imin) and differ
 413 slightly for the unreconstructed dataset CMST2.0-Nrec (Figure 9a & 9b). The warming of CMST-
 414 Nrec in Figure 9b is significantly lower than ~~that~~ that in Figure 9a ~~and~~, which is related to the lower
 415 land coverage. The LSAT coverage of CMST2.0-Nrec ~~was-is~~ low in previous decades, which is
 416 below 18% before 1900 (Fig. 3), so the GMST series is susceptible to the influence of ocean
 417 temperature, making the GMST series high; The LSAT coverage of CMST2.0-Nrec has increased
 418 in recent decades, with terrestrial coverage above 70% (Figure 3), but the coverage is low at high
 419 latitudes, in South America and Africa, where the absence of LSAT, especially at high latitudes and
 420 in the Arctic, makes the GMST series low. It can be seen that the warming rate of CMST2.0-Nrec

421 calculated using latitude-weighting will be significantly lower, so we are using the sea-land ratio
 422 method to calculate the warming trend when comparing each dataset in the following.

423 In Figure 9a, the CMST-Interim, CMST2.0-Imax and CMST2.0-Imin GMST series are lower
 424 than CMST-Nrec before the 1880s, which is mainly due to the lower coverage of observations in
 425 this period, making the interannual variability of the GMST series in CMST2.0-Nrec larger, while
 426 the reconstructed datasets filled in part of the default grids, resulting in higher coverage and thus
 427 lower interannual variability of GMST series. The reconstructed datasets show high agreement with
 428 the CMST-Nrec temperature series and its interannual variability as the coverage of the observations
 429 increased after the 1880s. While the GMST series of CMST2.0-Imax is significantly higher than the
 430 other three datasets after the 2000s because CMST2.0-Imax reconstructs the Arctic region and the
 431 polar amplification effect of the Arctic significantly increases the GMST series, the GMST series of
 432 CMST-Interim and CMST2.0-Imin are essentially the same as CMST-Nrec, but CMST2.0-Imin is
 433 slightly higher than CMST-Interim because CMST2.0-Imin fills the 80°N-90°N region with ice
 434 surface temperatures, while CMST-Interim uses SST. The GMST series of CMST2.0-Imax and
 435 CMST2.0-Imin are higher than CMST-Interim after 2000, indicating that the influence of polar
 436 temperature on global temperature also increases with global warming. In summary, the warming
 437 trends of the reconstructed datasets for 1850-2020 are all higher than CMST2.0-Nrec
 438 ($0.05 \pm 0.003^\circ\text{C}/10\text{a}(10\text{ yr})^{-1}$), with CMST2.0-Imax having the most significant warming trend
 439 ($0.054 \pm 0.003^\circ\text{C}/10\text{a}(10\text{ yr})^{-1}$) and CMST2.0-Imin the second largest ($0.053 \pm 0.003^\circ\text{C}/10\text{a}(10\text{ yr})^{-1}$)
 440 (Table 34). The warming trend estimated by CMST-Interim is $0.051 \pm 0.003^\circ\text{C}/10\text{a}(10\text{ yr})^{-1}$, which
 441 is slightly larger than CMST-Nrec, mainly due to the lower temperature series before the 1880s,
 442 excluding this period, the warming trend from 1880 to 2020 estimated by CMST-Interim ($0.073 \pm$
 443 $0.003^\circ\text{C}/10\text{a}(10\text{ yr})^{-1}$) is consistent with CMST-Nrec ($0.073 \pm 0.004^\circ\text{C}/10\text{a}(10\text{ yr})^{-1}$) (Table 4).
 444 While the warming trends of CMST2.0-Imax and CMST2.0-Imin are higher than the previous two
 445 datasets, $0.076 \pm 0.004^\circ\text{C}/10\text{a}(10\text{ yr})^{-1}$ and $0.074 \pm 0.003^\circ\text{C}/10\text{a}(10\text{ yr})^{-1}$ (Table 34), respectively, due
 446 to the polar amplification effect.

447 **6. Comparison of CMST2.0-Imax and CMST2.0-Imin with other datasets**

448 **Table 3 General information of input datasets**

	<u>Period of record</u>	<u>Land component</u>	<u>SST component</u>	<u>resolution</u>	<u>Interpolation, reconstruction and uncertainties evaluation</u>
<u>China-MST2.0</u>	1850-2020	<u>China-LSAT2.0</u>	ERSSTv5	5° × 5°	Spatial smoothing and EOTs; observational constraint; ensemble uncertainties Gaussian process method;
<u>HadCRUT5</u>	1850-2020	CRUTEM5	HadSST4	5° × 5°	observational constraint; ensemble uncertainties
<u>NOAAGlobal-Interim</u>	1850-2020	GHCNv4	ERSSTv5	5° × 5°	Spatial smoothing and EOTs; ensemble uncertainties
<u>GISTEMP v4</u>	1880-2020	GHCNv4	ERSSTv5	2° × 2°	Spatial interpolation methods over reasonable distances; ensemble uncertainties
<u>Berkelev Earth</u>	1850-2020	Berkeley	HadSST4	1° × 1°	Kriging-based spatial interpolation with constant

设置了格式: 上标
 设置了格式: 上标
 设置了格式: 上标
 设置了格式: 上标
 设置了格式: 上标
 设置了格式: 上标
 设置了格式: 上标
 设置了格式: 上标

设置了格式: 字体: 小五
 设置了格式: 字体: 小五
 设置了格式: 字体: 小五
 设置了格式: 字体: 小五
 设置了格式: 字体: 小五
 设置了格式: 字体: 小五

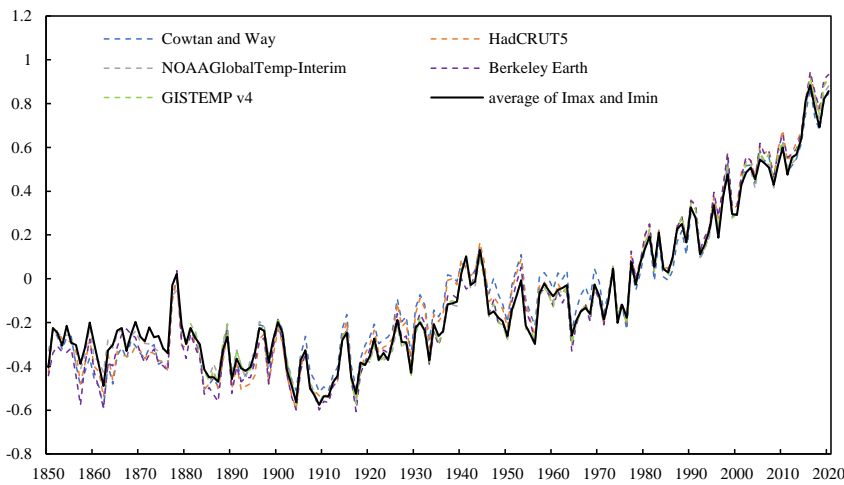
449

[Cowtan and Way](#) 1850-2020 CRUTEM4 HadSST3 $5^\circ \times 5^\circ$ [Kriging-based method with constant distance parameters at all latitudes](#)

[distance parameters at all latitudes](#)

[Kriging-based method with constant distance parameters at all latitudes](#)

设置了格式: 字体: 小五



450

451 Figure 10 Comparison of GMST anomalies series (relative to 1961-1990 average) for different
 452 datasets. The GMST anomalies series is the mean of global mean LSAT and SST weighted the
 453 proportion of land and sea. The average of Imax and Imin is the average of GMST series of
 454 CMST2.0-Imax and CMST2.0-Imin.

455 Figure 10 shows the GMST series of CMST2.0 compared with the other datasets (Table 3).
 456 The GMST series of the seven datasets (CMST2.0 includes two variants of Imax and Imin) are
 457 generally consistent. The GMST series of CMST2.0-Imax and CMST2.0-Imin are similar to the
 458 other five datasets, indicating that their estimated Arctic temperature variation is consistent with the
 459 other datasets, and can accurately reflect the impact of the Arctic amplification effect on GST. Due
 460 to sparse observations, the variability between datasets is high until the 1880s, as is the interannual
 461 variability between datasets. After the 1900s, the GMST series of CMST2.0-Imax and CMST2.0-
 462 Imin are generally lower than other datasets. In the 1910s-1970s, the Cowtan-Way dataset is
 463 consistently higher than other datasets. In the 1930s-1950s, HadCRUT5 is higher than the other
 464 datasets, but similar to Cowtan-Way. After the 2000s, the CMST2.0 datasets are generally lower
 465 than other datasets, with CMST2.0-Imax being closer to the NOAAglobalTemp-Interim GMST
 466 series. For the period 1850-2020, the warming trend of CMST2.0-Nrec is the lowest
 467 $(0.05 \pm 0.003^\circ\text{C}/10\text{a}(10\text{ yr})^{-1})$ and the highest $(0.062 \pm 0.003^\circ\text{C}/10\text{a}(10\text{ yr})^{-1})$ warming trend is
 468 Berkeley in the seven datasets. The warming trend of CMST-Interim is consistent with HadCRUT5,
 469 both at $0.051 \pm 0.003^\circ\text{C}/10\text{a}(10\text{ yr})^{-1}$. The warming trend of CMST2.0-Imax is the same as
 470 NOAAglobalTemp-Interim $(0.054 \pm 0.003^\circ\text{C}/10\text{a}(10\text{ yr})^{-1})$. Between 1880 and 2020, CMST2.0-Nrec
 471 $(0.073 \pm 0.004^\circ\text{C}/10\text{a}(10\text{ yr})^{-1})$ is agreement with CMST-Interim $(0.073 \pm 0.003^\circ\text{C}/10\text{a}(10\text{ yr})^{-1})$,
 472 CMST2.0-Imax is consistent with NOAAglobalTemp-Interim $(0.076 \pm 0.004^\circ\text{C}/10\text{a}(10\text{ yr})^{-1})$, and

设置了格式: 上标

设置了格式: 上标

设置了格式: 上标

设置了格式: 上标

设置了格式: 上标

设置了格式: 上标

设置了格式: 上标

473 CMST2.0-Imin ($0.075 \pm 0.003^{\circ}\text{C}/10\text{a}(10\text{ yr})^{-1}$) is consistent with Cowtan -Way
474 ($0.074 \pm 0.003^{\circ}\text{C}/10\text{a}(10\text{ yr})^{-1}$) (Table 34). We also calculate the warming trends of different datasets
475 for different periods 1900-2020, 1951-2020, 1979-2020 and 1998-2020 and found that the warming
476 rate becomes faster over time for most of the datasets, especially the increasing warming trend for
477 1998-2020 is much larger than the other periods, indicating that the global warming rate is
478 accelerating. The maximum warming trend of $0.228 \pm 0.029^{\circ}\text{C}/10\text{a}(10\text{ yr})^{-1}$ (GISTEMP v4) during
479 1998-2020 increased by $0.037 \pm 0.017^{\circ}\text{C}/10\text{a}(10\text{ yr})^{-1}$ compared to the warming trend during 1979-
480 2020. ~~the~~ The largest increasing warming trend is NOAA globalTemp-Interim, with a warming trend
481 of $0.037 \pm 0.017^{\circ}\text{C}/10\text{a}(10\text{ yr})^{-1}$ for 1998-2020, which is $0.04^{\circ}\text{C}/10\text{a}(10\text{ yr})^{-1}$ higher than the
482 warming trend during 1979-2020, followed by CMST2.0-Imax, CMST2.0-Imin and Berkeley Earth,
483 CMST2.0-Nrec and CMST-Interim have relatively small increases in the warming trend. The
484 relatively large increases of warming trend estimated in most datasets with reconstructed Arctic
485 temperatures, compared to those without (CMST2.0-Nrec and CMST-Interim), illustrate the impact
486 of polar amplification on global warming and reflect the importance of reconstructing Arctic default
487 data.
488

设置了格式: 上标

设置了格式: 上标

设置了格式: 上标

设置了格式: 上标

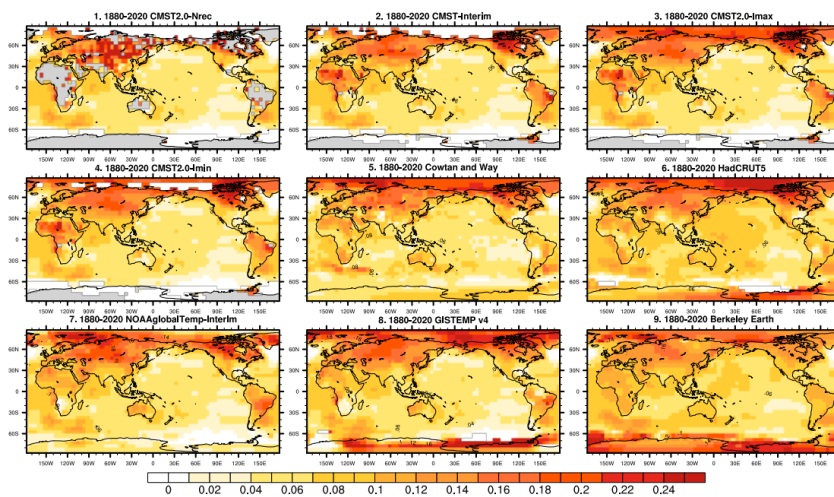
设置了格式: 上标

设置了格式: 上标

489 Table 43 Warming trends for different datasets during different periods. The GMST series used to
 490 calculate the warming trend is the mean of global mean LSAT and SST weighted the proportion of
 491 land and sea.

	CMST2.0 -Nrec	CMST2.0 -Interim	CMST2.0- Imax	CMST-Imin	Cowtan - Way	HadCRUT5	NOAAglobal Temp-Interim	Berkeley Earth	GISTEM P v4
1850-2020	0.050±0.003	0.051±0.003	0.054±0.00 3	0.053±0.003	0.058±0.003	0.051±0.003	0.054±0.003	0.062±0.003	—
1880-2020	0.073±0.004	0.073±0.003	0.076±0.00 4	0.075±0.003	0.074±0.003	0.081±0.004	0.076±0.004	0.083±0.004	0.077±0.004
1900-2020	0.091±0.004	0.090±0.004	0.093±0.00 4	0.091±0.004	0.084±0.004	0.094±0.004	0.093±0.004	0.099±0.004	0.095±0.004
1951-2020	0.145±0.007	0.139±0.007	0.146±0.00 7	0.143±0.007	0.130±0.008	0.150±0.008	0.147±0.007	0.155±0.008	0.151±0.007
1979-2020	0.174±0.013	0.168±0.011	0.184±0.01 1	0.179±0.011	0.190±0.012	0.193±0.012	0.184±0.012	0.195±0.012	0.191±0.012
1998-2020	0.198±0.030	0.192±0.027	0.212±0.02 6	0.209±0.026	0.189±0.028	0.215±0.028	0.224±0.028	0.220±0.030	0.228±0.029

492



493
 494

Figure 11 Distribution of warming trends estimated from different datasets during 1880-2020.

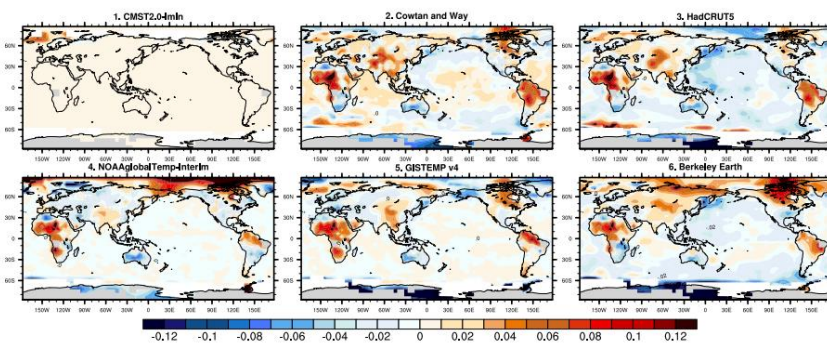


Figure 12 Differences in warming trends estimated by other 6 datasets (including CMST2.0-Imin) and CMST2.0-Imax

Figure 11 compares the distribution of warming trends for different datasets for 1880-2020. The distribution of warming trends is relatively consistent among the nine datasets except for the Antarctic, with a zone of high warming values in central Asia and Europe, and northeastern North America. There are large differences among the datasets in the Antarctic region due to the sparse observations. CMST-Interim, CMSR2.0-Imax and CMST2.0-Min-Imin have fewer LSATs in the Antarctic due to the sparse observations and observational constraints. Except for CMST2.0-Nrec, the estimated warming trends of the other eight datasets have a clear trend of increasing clearly increase with latitude in the Northern Hemisphere region. Most datasets assess a significantly higher warming trend in the Arctic (60°N-90°N) than in the lower latitudes. Except for the CMST2.0-Nrec and CMST-Interim datasets in which Arctic temperature is not available, the magnitude of the estimated Arctic warming trend for 1880-2020 is similar (Figure 12). Still, the warming trends near the poles differ significantly, with more significant warming trends estimated by HadCRUT5 and GISTEMP v4. CMST2.0-Imax, CMST2.0-Imin, Cowtan-Way and Berkeley Earth have similar warming trends, while NOAAglobalTemp-Interim has the smallest warming estimate near the poles. CMST2.0-Imax, HadCRUT5, and GISTEMP v4 all show a high warming trend in the high latitudes of North America and the northwestern Arctic Ocean, but CMST2.0-Imax has a relatively small range of highs. Cowtan-Way and Berkeley Earth are similar to the former three datasets, but with but have smaller ranges and magnitudes. Meanwhile, each dataset also has a range of warming highs in the southeastern Arctic Ocean, NOAAglobalTemp-Interim estimates the most extensive range of warming, CMST2.0-Imax, CMST2.0-Min, HadCRUT5, and GISTEMP v4 estimate similar ranges of warming. In addition, all datasets, including CMST2.0-Nrec and CMST-Interim, have low warming trend near Scandinavia. The analysis of the warming trends in the Arctic shows that the magnitude and spatial distribution of the warming trends estimated based on CMST2.0-Imax and CMST-Imin are more consistent with the other datasets. Therefore they are reasonable for the spatial interpolation reconstruction of temperature anomalies in the Arctic.

7. Summary and Prospects

This paper describes the composition and construction process of the latest versions of the C-LSAT 2.0 and CMST 2.0 ensemble datasets. The C-LSAT 2.0 datasets consist of the C-LSAT 2.0 gridded dataset and the reconstructed C-LSAT 2.0 dataset, including three meteorological elements: monthly average, maximum and minimum temperatures. The CMST2.0 datasets consist of the

528 CMST 2.0-Nrec gridded dataset and two reconstructed datasets (including CMST 2.0-Imax and
529 CMST2.0-Imin). The CMST 2.0 datasets contain the monthly average temperature anomaly. The
530 resolution of all datasets is $5^{\circ}\times 5^{\circ}$ and the time range is 1850-2020. The reconstructed C-LSAT 2.0
531 dataset, reconstructed according to the high- and low-frequency reconstruction method in Sun et al.
532 (2021), is merged with ERSSTv5 to generate the global surface temperature ensemble dataset
533 CMST-Interim. CMST 2.0-Imax and CMST 2.0-Imin are based on CMST-Interim, combining
534 Δ IDW and high- and low-frequency reconstruction methods for temperature reconstruction in the
535 Arctic. Compared with the unreconstructed dataset CMST-2.0-Nrec, the coverage of the
536 reconstructed datasets is greatly improved. These two datasets have greatly improved coverage in
537 the Northern Hemisphere due to the reconstruction in the Arctic. Compared to 60%-70% for CMST
538 2.0-Nrec before 1910, the coverage of CMST-Interim has improved to 75%-85%, and CMST 2.0-
539 Imax and CMST 2.0-Imin are both above 80%. The coverage of CMST 2.0-Imax and CMST2.0-
540 Imin in the Northern Hemisphere is 80%-99% and CMST-Interim is 65%-87%. In the Southern
541 Hemisphere, there was no difference in coverage between the three reconstructed datasets
542 There was no difference in coverage between the three reconstructed datasets in the Southern Hemisphere.

543 We then systematically evaluate the uncertainty of the reconstructed datasets. The results of
544 the uncertainty assessment of the reconstructed C-LSAT-2.0 show that the magnitude of the
545 reconstruction uncertainty is generally smaller than that of the parameter uncertainty, and the
546 parameter uncertainty mainly determines the total uncertainty of the LSAT. The uncertainty of the
547 reconstructed LSAT is similar to previous estimates (Li et al., 2020; Sun et al., 2021). The
548 uncertainty of reconstructed C-LSAT2.0+Imax and reconstructed C-LSAT2.0+Imin is relatively
549 consistent with the uncertainty variation of reconstructed C-LSAT2.0, but the interannual variation
550 is larger, and the increasing trend of parameter uncertainty of reconstructed C-LSAT2.0+Imax
551 and reconstructed C-LSAT2.0+Imin is significantly higher than that of reconstructed C-LSAT2.0 after
552 2017. The uncertainty analysis of CMST 2.0 shows that the uncertainty of GST depends mainly on
553 the oceanic component before 1986, is determined by both oceanic and terrestrial components
554 during 1986-2003, and depends on the magnitude of the terrestrial component after 2003.

555 Results comparing the GMST series of the three CMST 2.0 datasets and CMST-Interim show
556 that the reconstructed datasets improve the estimation of global warming trends while increasing
557 data coverage, especially for the datasets that include the Arctic region in the reconstructed area.
558 Compared with $0.05 \pm 0.003^{\circ}\text{C}/10\text{a}(10\text{ yr})^{-1}$ and $0.073 \pm 0.004^{\circ}\text{C}/10\text{a}(10\text{ yr})^{-1}$ for CMST 2.0-Nrec,
559 CMST 2.0-Imax and CMST 2.0-Imin estimated warming trends of $0.054 \pm 0.003^{\circ}\text{C}/10\text{a}(10\text{ yr})^{-1}$ and
560 $0.053 \pm 0.003^{\circ}\text{C}/10\text{a}(10\text{ yr})^{-1}$ for 1850 -2020 and 1880 -2020 is $0.076 \pm 0.004^{\circ}\text{C}/10\text{a}(10\text{ yr})^{-1}$ and
561 $0.075 \pm 0.003^{\circ}\text{C}/10\text{a}(10\text{ yr})^{-1}$, with a very significant increase. Compared with the five datasets in
562 IPCC AR6, it can be found that the datasets considering the reconstruction of Arctic sea ice
563 temperature can more accurately reflect the effect of polar amplification on global temperature, and
564 the GMST series and warming trends estimated by CMST 2.0-Imax and CMST 2.0-Imin are more
565 consistent with these five datasets, and b. The GMST series and warming trends estimated by CMST
566 2.0-Imax and CMST 2.0-Imin are more consistent with these five datasets. Both have similar
567 estimates of the spatial distribution and magnitude of warming trends in the Arctic as the other
568 datasets.

569 The current CMST 2.0 dataset for the Arctic is a reconstruction of the sea ice surface
570 temperature in a defined region ($65^{\circ}\text{N}-90^{\circ}\text{N}$ or $80^{\circ}\text{N}-90^{\circ}\text{N}$) with 2 meters air temperature. Although
571 the influence of Arctic temperature on global temperature is considered and the change of GMST

设置了格式: 上标

设置了格式: 上标

设置了格式: 上标

设置了格式: 上标

设置了格式: 上标

设置了格式: 上标

572 series is estimated relatively accurately, it still cannot reflect the impact of sea ice dynamics on
573 global temperature very accurately. Therefore, our future work will gradually consider the dynamics
574 of sea ice as much as possible in the reconstruction process in order to more accurately estimate and
575 analyze the amplification effect of the Arctic and its impact on GMST.

576 Last but not ~~the~~ least, due to the limited observations, it is very difficult to fully reconstruct the
577 SATs over the Antarctic and the surrounding SSTs during the earlier periods (for example: prior to
578 ~~the~~ 1950s), which made the CMST2.0 is still not “fully” coverage. This will need to be better
579 addressed by continuing to supplement data sources and ~~refining technical~~technical refining
580 methods in future studies.

581 8. Data availability

582 The C-LSAT2.0 datasets are currently publicly available at the website of figshare under the
583 DOI <https://doi.org/10.6084/m9.figshare.16968334.v4> (Sun and Li, 2021b), which contains
584 monthly mean, maximum and minimum temperature before and after reconstruction during 1850-
585 2020.-

586 The CMST2.0 datasets can be downloaded at
587 <https://doi.org/10.6084/m9.figshare.16929427.v4> (Sun and Li, 2021a), which contains CMST2.0-
588 Nrec, CMST-Interim, CMST2.0-Imax and CMST2.0-Imin datasets.

589 ~~Both of~~These datasets are also available freely at: [http:// www.gwpu.net](http://www.gwpu.net).

590

591 **Author contributions.** All co-authors were involved in data collection, data analysis, and dataset
592 development. QL was primarily responsible for writing the paper and constructing the dataset. QL
593 and WS conceived the study design with the participation of all co-authors. All authors were
594 involved in the writing of the paper.

595

596 **Competing interests.** The authors declare that they have no conflict of interest.

597

598 **Acknowledgments.** This study is supported by the Natural Science Foundation of China (Grant:
599 41975105) , the National Key R&D Program of China (Grant: 2018YFC1507705;
600 2017YFC1502301).

601

602

603

Reference

604 [Brohan, P., Kennedy, J. J., Harris, I., Tett, S. F. B., and Jones, P. D.: Uncertainty estimates in regional](#)
605 [and global observed temperature changes: A new data set from 1850, Journal of Geophysical](#)
606 [Research: Atmospheres, 111, 2006.](#)

607 [Cheng, J., Li, Q., Chao, L., Maity, S., Huang, B., and Jones, P.: Development of High Resolution](#)
608 [and Homogenized Gridded Land Surface Air Temperature Data: A Case Study Over Pan-East Asia,](#)
609 [Frontiers in Environmental Science, 8, 2020.](#)

610 [Cowtan, K. and Way, R. G.: Coverage bias in the HadCRUT4 temperature series and its impact on](#)
611 [recent temperature trends, Quarterly Journal of the Royal Meteorological Society, 140, 1935-1944,](#)
612 [2014.](#)

613 [Dai, A., Luo, D., Song, M., and Liu, J.: Arctic amplification is caused by sea-ice loss under](#)

带格式的: 缩进: 首行缩进: 2 字符

带格式的: 正文

设置了格式: 字体: (默认) Times New Roman, 检查拼写和语法

614 increasing CO₂, *Nature Communications*, 10, 2019.

615 Freeman, E., Woodruff, S. D., Worley, S. J., Lubker, S. J., Kent, E. C., Angel, W. E., Berry, D. I.,
616 Brohan, P., Eastman, R., Gates, L., Gloeden, W., Ji, Z., Lawrimore, J., Rayner, N. A., Rosenhagen,
617 G., and Smith, S. R.: ICOADS Release 3.0: a major update to the historical marine climate record,
618 *International Journal of Climatology*, 37, 2211-2232, 2017.

619 Goosse, H., Kay, J. E., Armour, K. C., Bodas-Salcedo, A., Chepfer, H., Docquier, D., Jonko, A.,
620 Kushner, P. J., Lecomte, O., Massonnet, F., Park, H.-S., Pithan, F., Svensson, G., and Vancoppenolle,
621 M.: Quantifying climate feedbacks in polar regions, *Nature Communications*, 9, 2018.

622 Gulev, S. K., Thorne, P. W., Ahn, J., Dentener, F. J., Domingues, C. M., Gerland, S., Gong, D.,
623 Kaufman, D. S., C. H., and Nnamchi, J. Q. J. A.: Changing State of the Climate System. In *Climate*
624 *Change 2021: The Physical Science Basis. Contribution of Working Group I to the Sixth Assessment*
625 *Report of the Intergovernmental Panel on Climate Change [MassonDelmotte, V., P. Zhai, A. Pirani,*
626 *S.L. Connors, C. Péan, S. Berger, N. Caud, Y. Chen, L. Goldfarb, M.I. Gomis, M. Huang, K. Leitzell,*
627 *E. Lonnoy, J.B.R. Matthews, T.K. Maycock, T. Waterfield, O. Yelekçi, R. Yu, and B. Zhou (eds.)].*
628 *Cambridge University Press. In Press, 2021.*

629 Hansen, J., Ruedy, R., Sato, M., and Lo, K.: GLOBAL SURFACE TEMPERATURE CHANGE,
630 *Reviews of Geophysics*, 48, 2010.

631 Hershbach, H., Bell, B., Berrisford, P., Hirahara, S., Horányi, A., Muñoz-Sabater, J., Nicolas, J.,
632 Peubey, C., Radu, R., Schepers, D., Simmons, A., Soci, C., Abdalla, S., Abellan, X., Balsamo, G.,
633 Bechtold, P., Biavati, G., Bidlot, J., Bonavita, M., De Chiara, G., Dahlgren, P., Dee, D., Diamantakis,
634 M., Dragani, R., Flemming, J., Forbes, R., Fuentes, M., Geer, A., Haimberger, L., Healy, S., Hogan,
635 R. J., Hólm, E., Janisková, M., Keeley, S., Laloyaux, P., Lopez, P., Lupu, C., Radnoti, G., de Rosnay,
636 P., Rozum, I., Vamborg, F., Villaume, S., and Thépaut, J.-N.: The ERA5 global reanalysis, *Quarterly*
637 *Journal of the Royal Meteorological Society*, 146, 1999-2049, <https://doi.org/10.1002/qj.3803>, 2020.

638 Huang, B., Thorne, P. W., Smith, T. M., Liu, W., Lawrimore, J., Banzon, V. F., Zhang, H.-M.,
639 Peterson, T. C., and Menne, M.: Further Exploring and Quantifying Uncertainties for Extended
640 Reconstructed Sea Surface Temperature (ERSST) Version 4 (v4), *Journal of Climate*, 29, 3119-3142,
641 2016.

642 Huang, B., Thorne, P. W., Banzon, V. F., Boyer, T., Chepurin, G., Lawrimore, J. H., Menne, M. J.,
643 Smith, T. M., Vose, R. S., and Zhang, H.-M.: Extended Reconstructed Sea Surface Temperature,
644 Version 5 (ERSSTv5): Upgrades, Validations, and Intercomparisons, *Journal of Climate*, 30, 8179-
645 8205, 2017.

646 Huang, B., Menne, M. J., Boyer, T., Freeman, E., Gleason, B. E., Lawrimore, J. H., Liu, C., Rennie,
647 J. J., Schreck, C. J., Sun, F., Vose, R., Williams, C. N., Yin, X., and Zhang, H.-M.: Uncertainty
648 Estimates for Sea Surface Temperature and Land Surface Air Temperature in NOAA GlobalTemp
649 Version 5, *Journal of Climate*, 33, 1351-1379, 2020.

650 Jones, P. D., Osborn, T. J., and Briffa, K. R.: Estimating Sampling Errors in Large-Scale Temperature
651 Averages, *Journal of Climate*, 10, 2548-2568, 1997.

652 Kadow, C., Hall, D. M., and Ulbrich, U.: Artificial intelligence reconstructs missing climate
653 information, *Nature geoscience*, 13, 408-413, 2020.

654 Kent, E. C., Kennedy, J. J., Smith, T. M., Hirahara, S., Huang, B., Kaplan, A., Parker, D. E., Atkinson,
655 C. P., Berry, D. I., and Carella, G.: A call for new approaches to quantifying biases in observations
656 of sea surface temperature, *Bulletin of the American Meteorological Society*, 98, 1601-1616, 2017.

657 Latonin, M. M., Bashmachnikov, I. L., Bobylev, L. P., and Davy, R.: Multi-model ensemble mean

658 of global climate models fails to reproduce early twentieth century Arctic warming, *Polar Science*,
659 100677, 2021.

660 Lenssen, N. J. L., Schmidt, G. A., Hansen, J. E., Menne, M. J., Persin, A., Ruedy, R., and Zyss, D.:
661 Improvements in the GISTEMP Uncertainty Model, *Journal of Geophysical Research: Atmospheres*,
662 124, 6307-6326, 2019.

663 Li, Q., Sun, W., Huang, B., Dong, W., Wang, X., Zhai, P., and Jones, P.: Consistency of global
664 warming trends strengthened since 1880s, *Science Bulletin*, 65, 1709-1712, 2020.

665 Li, Q., Sun, W., Yun, X., Huang, B., Dong, W., Wang, X. L., Zhai, P., and Jones, P.: An updated
666 evaluation of the global mean land surface air temperature and surface temperature trends based on
667 CLSAT and CMST, *Climate Dynamics*, 56, 635-650, 2021.

668 Li, Q., Sheng, B., Huang, J., Li, C., Song, Z., Chao, L., Sun, W., Yang, Y., Jiao, B., Guo, Z., Liao,
669 L., Li, X., Sun, C., Li, W., Huang, B., Dong, W., and Jones, P.: Different climate response persistence
670 causes warming trend unevenness at continental scales, *Nature Climate Change*, s41558-022-
671 01313-9, [in press](#), 2022.

672 Lu, J. and Cai, M.: Seasonality of polar surface warming amplification in climate simulations,
673 *Geophysical Research Letters*, 36, 2009.

674 Lu, J. and Cai, M.: Quantifying contributions to polar warming amplification in an idealized coupled
675 general circulation model, *Climate Dynamics*, 34, 669-687, 2010.

676 Menne, M. J., Williams, C. N., Gleason, B. E., Rennie, J. J., and Lawrimore, J. H.: The global
677 historical climatology network monthly temperature dataset, version 4, *Journal of Climate*, 31,
678 9835-9854, 2018.

679 Morice, C. P., Kennedy, J. J., Rayner, N. A., and Jones, P. D.: Quantifying uncertainties in global
680 and regional temperature change using an ensemble of observational estimates: The HadCRUT4
681 data set, *Journal of Geophysical Research: Atmospheres*, 1, 1-13, 2012.

682 Morice, C. P., Kennedy, J. J., Rayner, N. A., Winn, J. P., Hogan, E., Killick, R. E., Dunn, R. J. H.,
683 Osborn, T. J., Jones, P. D., and Simpson, I. R.: An updated assessment of near-surface temperature
684 change from 1850: the HadCRUT5 dataset (in press), *Journal of Geophysical Research*
685 (*Atmospheres*), 2021.

686 Parker, D. E.: A demonstration that large-scale warming is not urban, *Journal of climate*, 19, 2882-
687 2895, 2006.

688 Parker, D. E., Jones, P. D., Folland, C. K., and Bevan, A.: Interdecadal changes of surface
689 temperature since the late nineteenth century, *Journal of Geophysical Research: Atmospheres*, 99,
690 14373-14399, 1994.

691 Rohde, R., Muller, R., Jacobsen, R., Perlmutter, S., Rosenfeld, A., Wurtele, J., Curry, J., Wickham,
692 C., and Mosher, S.: Berkeley earth temperature averaging process, *Geoinformatics & Geostatistics:*
693 *An Overview*, 1, 1-13, 2013a.

694 Rohde, R., Muller, R. A., Jacobsen, R., Muller, E., Perlmutter, S., Rosenfeld, A., Wurtele, J., Groom,
695 D., and Wickham, C.: A New Estimate of the Average Earth Surface Land Temperature Spanning
696 1753 to 2011, *Geoinfor Geostat: An Overview*, 1, 1-7, 2013b.

697 Rohde, R. A. and Hausfather, Z.: The Berkeley Earth Land/Ocean Temperature Record, *Earth*
698 *System Science Data*, 12, 3469-3479, 2020.

699 Sun, W. and Li, Q.: China global Merged surface temperature 2.0 during 1850-2020,
700 10.6084/m9.figshare.16929427.v4, 2021a.

701 Sun, W. and Li, Q.: China global Land Surface Air Temperature 2.0 during 1850-2020,

设置了格式: 字体: (默认) Times New Roman, 检查拼写和语法

702 10.6084/m9.figshare.16968334.v4, 2021b.
703 Sun, W., Li, Q., Huang, B., Cheng, J., Song, Z., Li, H., Dong, W., Zhai, P., and Jones, P.: The
704 Assessment of Global Surface Temperature Change from 1850s: The C-LSAT2.0 Ensemble and the
705 CMST-Interim Datasets, *Advances in Atmospheric Sciences*, 38, 875-888, 2021.
706 Thorne, P. W., Willett, K. M., Allan, R. J., Bojinski, S., Christy, J. R., Fox, N., Gilbert, S., Jolliffe,
707 I., Kennedy, J. J., Kent, E., Tank, A. K., Lawrimore, J., Parker, D. E., Rayner, N., Simmons, A.,
708 Song, L., Stott, P. A., and Trewin, B.: Guiding the Creation of A Comprehensive Surface
709 Temperature Resource for Twenty-First-Century Climate Science, *Bulletin of the American
710 Meteorological Society*, 92, ES40-ES47, 10.1175/2011bams3124.1, 2011.
711 Trewin, B. C.: Techniques involved in developing the Australian Climate Observations Reference
712 Network – Surface Air Temperature (ACORN-SAT) dataset, CAWCR Technical Report 49, Centre
713 for Australian Weather and Climate Research, Melbourne, 2012.
714 Vose, R. S., Huang, B., Yin, X., Arndt, D., Easterling, D. R., Lawrimore, J. H., Menne, M. J.,
715 Sanchez Lugo, A., and Zhang, H. M.: Implementing Full Spatial Coverage in NOAA's Global
716 Temperature Analysis, *Geophysical Research Letters*, 48, 2021.
717 Vose, R. S., Arndt, D., Banzon, V. F., Easterling, D. R., Gleason, B., Huang, B., Kearns, E.,
718 Lawrimore, J. H., Menne, M. J., and Peterson, T. C.: NOAA's merged land-ocean surface
719 temperature analysis, *Bulletin of the American Meteorological Society*, 93, 1677-1685, 2012.
720 Wang, J., Xu, C., Hu, M., Li, Q., Yan, Z., and Jones, P.: Global land surface air temperature dynamics
721 since 1880, *International Journal of Climatology*, 38, e466-e474, <https://doi.org/10.1002/joc.5384>,
722 2018.
723 Xiao, H., Zhang, F., Miao, L., Liang, X. S., Wu, K., and Liu, R.: Long-term trends in Arctic surface
724 temperature and potential causality over the last 100 years, *Climate Dynamics*, 55, 1443-1456, 2020.
725 Xu, W., Li, Q., Jones, P., Wang, X. L., Trewin, B., Yang, S., Zhu, C., Zhai, P., Wang, J., Vincent, L.,
726 Dai, A., Gao, Y., and Ding, Y.: A new integrated and homogenized global monthly land surface air
727 temperature dataset for the period since 1900, *Climate Dynamics*, 50, 2513-2536, 2018.
728 Yamanouchi, T.: Early 20th century warming in the Arctic: A review, *Polar Science*, 5, 53-71, 2011.
729 Yun, X., Huang, B., Cheng, J., Xu, W., Qiao, S., and Li, Q.: A new merge of global surface
730 temperature datasets since the start of the 20th century, *Earth System Science Data*, 11, 1629-1643,
731 2019.
732 Zhang, H. M., Lawrimore, J., Huang, B., Menne, M. J., Yin, X., Sánchez-Lugo, A., Gleason, B. E.,
733 Vose, R., Arndt, D., and Rennie, J. J.: Updated temperature data give a sharper view of climate
734 trends, *Eos*, 100, 1961-2018, 2019.
735

带格式的: 缩进: 左侧: 0 厘米, 首行缩进: 0 字符